

Forecasting Generative Amplification

Henning Bahl¹, Sascha Diefenbacher², Nina Elmer¹, Tilman Plehn^{1,3}, and Jonas Spinner¹

¹ Institut für Theoretische Physik, Universität Heidelberg, Germany

² Physics Division, Lawrence Berkeley National Laboratory, Berkeley, USA

³ Interdisciplinary Center for Scientific Computing (IWR), Universität Heidelberg, Germany

September 11, 2025

Abstract

Generative networks are perfect tools to enhance the speed and precision of LHC simulations. It is important to understand their statistical precision, especially when generating events beyond the size of the training dataset. We present two complementary methods to estimate the amplification factor without large holdout datasets. Averaging amplification uses Bayesian networks or ensembling to estimate amplification from the precision of integrals over given phase-space volumes. Differential amplification uses hypothesis testing to quantify amplification without any resolution loss. Applied to state-of-the-art event generators, both methods indicate that amplification is possible in specific regions of phase space, but not yet across the entire distribution.

Contents

1	Introduction	2
2	Basics	3
3	Averaging amplification factor	4
3.1	Metric extrapolation	5
3.2	1D Gaussian fit	6
3.3	Bayesian generative networks	8
3.4	Gaussian-ring toy data	9
4	Differential amplification factor	10
4.1	Kolmogorov-Smirnov test	11
4.2	Gaussian-ring toy data	13
5	Top pair production	16
5.1	Averaging amplification	17
5.2	Differential amplification	18
6	Outlook	20
	References	21

1 Introduction

The enormous amount of data at the Large Hadron Collider (LHC) has allowed us to explore the Standard Model with unprecedented precision. Over the next decade, the High Luminosity LHC (HL-LHC) will increase the amount of data by another order of magnitude, promising a significant jump in precision. To analyse this data will require a corresponding increase in the precision and the amount of simulation data.

LHC simulations rely on a comprehensive Monte Carlo (MC)-based simulation chain. It starts with the interaction of partons, from where the events are propagated through jet radiation and hadronization steps to the detector simulation. All steps are based on first principles, with a high level of precision. This link to proper physics models comes with significant computational costs. As a result, we expect the need for HL-LHC simulations to exceed our computational budget by a significant factor.

To solve this pressing problem, we need more efficient simulation methods. Modern machine learning (ML) provides such methods, including generative networks that learn the underlying phase space densities from a controlled dataset. For instance, we can train a generative network on classical simulation and use it to generate extra simulation data significantly faster. Such generative networks have been developed for event generation [1–6], hadronization [7, 8], detector simulation [9–13], and neural importance sampling [14–16]. In addition, these generative methods are complemented with parameterized fast simulation [17] and amplitude surrogates [18–21].

Generative fast simulation rests on the assumption that samples drawn from the network can exceed the statistical limitations of the training data, the so-called *amplification*^{*}. It has been shown to work for synthetic data [22–24] and for simulated physics data [25]. This amplification behavior goes back to the interpolation of the underlying density given the inductive bias of the generative network.

To quantify the amount of amplification, we have, until now, relied on knowing the true underlying distribution or on a large holdout dataset [22, 24, 25]. In actual physics applications with limited statistics, these approaches are not practical. In this work, we investigate methods to quantify amplification factors without knowledge of the true distribution. This way, we address two common concerns: first, knowing the amplification factor of a generative network provides an insight how to use the network for simulations; second, the amplification factor of a generative network provides a lower limit on the statistical uncertainty of a generated dataset. In that sense, reliable amplification is a vital part of generative uncertainty quantification.

The paper is structured as follows: In [Section 2](#) we introduce the fundamental concepts. In [Section 3](#) and [Section 4](#), we present results on the experimental setup for averaging and differential amplification, respectively. [Section 5](#) shows how our amplification estimates can be applied to state-of-the-art generative networks for top pair events at the LHC. [Section 6](#) presents our conclusions.

^{*}Earlier we have referred to this effect as GANplification. In this paper we will, strictly speaking, show that L-GATrification and LLoCa-Transformerification are much more successful. We therefore decide to retire the specific portmanteau.

2 Basics

In this section we very briefly review the idea of generative amplification and present our main toy dataset and network setup. All details about the physics application are given in [Section 5](#).

Amplification

Amplification means that a generated dataset provides a better description of the true underlying distribution than the training data. Let $p_{\text{true}}(x)$ be the probability density which the generative network should describe. We draw n_{train} training events, from which the generative network learns its density $p_{\text{gen}}(x)$,

$$D_{\text{true}}^{n_{\text{train}}} \sim p_{\text{true}}(x) \approx p_{\text{gen}}(x) \quad \text{with} \quad |D_{\text{true}}^{n_{\text{train}}}| = n_{\text{train}} . \quad (1)$$

Then, we sample events from this learned density, and amplification assumes that these events follow the true density rather than the training data

$$D_{\text{gen}}^{n_{\text{gen}}} \sim p_{\text{gen}}(x) \quad \text{versus} \quad D_{\text{gen}}^{n_{\text{gen}}} \stackrel{?}{\sim} p_{\text{true}}(x) . \quad (2)$$

Two effects determine the success of amplification:

1. no network training is perfect, so the learned $p_{\text{gen}}(x)$ will not reproduce $D_{\text{true}}^{n_{\text{train}}}$ perfectly;
2. $p_{\text{gen}}(x)$ will smooth out $D_{\text{true}}^{n_{\text{train}}}$, giving a better approximation to $p_{\text{true}}(x)$.

To determine the amount of amplification following [Eq. \(2\)](#), we need a metric to measure the agreement of a dataset D with a probability distribution $p(x)$. Given such a metric $M(D, p(x))$, we implicitly define the effective number of true samples in the hypothetically generated dataset, n_{equiv} , via

$$D_{\text{true}}^{n_{\text{equiv}}} \sim p_{\text{true}}(x) \quad \text{such that} \quad M(D_{\text{true}}^{n_{\text{equiv}}}, p_{\text{true}}(x)) \equiv M(D_{\text{gen}}^{n_{\text{gen}}}, p_{\text{true}}(x)) . \quad (3)$$

This defines the amplification factor

$$G = \frac{n_{\text{equiv}}}{n_{\text{train}}} . \quad (4)$$

Realistically, we do not have access to $p_{\text{true}}(x)$. In the past, large holdout datasets have been used to approximate $p_{\text{true}}(x)$, and combined with various ad-hoc metrics $M(D, p(x))$.

In this paper, we aim to estimate G without a large holdout dataset using two different approaches to define the metric $M(D, p(x))$, *averaging* amplification and *differential* amplification. Both methods are designed to not require information about the true distribution. When the true distribution is known analytically or implicitly available as a large holdout dataset, we use it to validate our two amplification estimates. We start with a toy setup with a simple data distribution and an interpretable generative network. After that, we apply both methods to a proper LHC simulation problem.

Toy dataset and network

As a toy dataset, we use a d -dimensional Gaussian ring distribution, with radial distribution

$$p_R(x) = \mathcal{N}(R; \mu, \sigma^2) \quad \text{with} \quad \mu = 1 , \quad \sigma = 0.1 , \quad (5)$$

and flat angular distributions $[p_{\phi,1}(x), \dots, p_{\phi,d-1}(x)]$. The networks are trained on Cartesian representation $[x_1, \dots, x_d]$, with $\sum_i x_i^2 = R^2$. We evaluate them in polar coordinates, to ensure that the network learns the $[x_1, \dots, x_d]$ -distributions and their correlations, to recover the correct R .

We parametrize the density using an autoregressive transformer [3]. It provides a combination of fast sampling with access to exact densities. We approximate the multi-dimensional phase space distribution as an autoregressive product of conditional probabilities

$$p(x_1, \dots, x_n) = p(x_1)p(x_2|x_1) \cdots p(x_n|x_1 \dots x_{n-1}). \quad (6)$$

The conditional probabilities $p(x_i|x_1 \dots x_{i-1})$ are one-dimensional and parametrized in terms of a Gaussian mixture

$$p(x_i|x_1 \dots x_{i-1}) = \sum_{j=1}^N w_j \mathcal{N}(x_i|\mu_j, \sigma_j). \quad (7)$$

The parameters w_j, μ_j, σ_j implicitly depend on the condition $(x_1 \dots x_{i-1})$, and the weights w_j sum to one. Evaluating this density is straightforward using the analytic expression, and sampling from this density can be done sequentially. The network is trained to minimize the negative log-likelihood

$$\mathcal{L} = \langle -\log p(x) \rangle_{x \sim p(x)} = \left\langle -\sum_{i=1}^n \log p(x_i|x_1 \dots x_{i-1}) \right\rangle_{x \sim p(x)}. \quad (8)$$

In each autoregressive step, we use a transformer architecture to predict the parameters $(w, \mu, \sigma)_i$ characterizing $p(x_i|x_1 \dots x_{i-1})$ conditioned on the prior phase space components $x_1 \dots x_{i-1}$. Specifically, we embed each component x_k as a transformer token, and extract a set of Gaussian mixture parameters from each token. The first set of mixture parameters $(w, \mu, \sigma)_1$ is predicted based on a dummy start token $x_0 = 0$.

3 Averaging amplification factor

Averaging amplification generalizes previous work to quantify amplification [24, 26]. Following Eq. (2), we want to quantify the agreement between a dataset $D_{\text{gen}}^{n_{\text{gen}}}$ with the probability density $p_{\text{true}}(x)$. For a given, arbitrary phase space volume V , our reference is the true-density integral

$$I(p_{\text{true}}) = \int_V dx p_{\text{true}}(x). \quad (9)$$

We compare the integral to the fraction of points of $D_{\text{gen}}^{n_{\text{gen}}}$ which lie in V ,

$$\bar{I}(D_{\text{gen}}^{n_{\text{gen}}}) = \frac{1}{n} \sum_{x \in D_{\text{gen}}^{n_{\text{gen}}}} \mathbf{1}_{x \in V} \quad \text{with} \quad \mathbf{1}_{x \in V} = \begin{cases} 1 & x \in V \\ 0 & \text{else} \end{cases}. \quad (10)$$

The deviation between the sample and the true density for a given V can be decomposed as

$$\begin{aligned} \sigma_{\text{true}}^2(D_{\text{gen}}^{n_{\text{gen}}}, p_{\text{true}}) &= \left\langle [I(p_{\text{true}}) - \bar{I}(D_{\text{gen}}^{n_{\text{gen}}})]^2 \right\rangle \\ &= \begin{cases} \sigma_{\text{stat}}^2(n_{\text{gen}}) & p_{\text{gen}} = p_{\text{true}} \\ \sigma_{\text{stat}}^2(n_{\text{gen}}) + \sigma_{\text{model}}^2(p_{\text{gen}}, p_{\text{true}}) & p_{\text{gen}} \neq p_{\text{true}} \end{cases}. \end{aligned} \quad (11)$$

Here, σ_{stat} is the statistical uncertainty, which does not vanish even when $p_{\text{gen}} = p_{\text{true}}$. The uncertainty due to mis-modelling p_{true} as p_{gen} is σ_{model} .

Using $\sigma_{\text{true}}(D_{\text{gen}}^{n_{\text{gen}}}, p_{\text{true}})$ as the metric introduced in Eq. (3), the implicit definition of n_{equiv} in Eq. (3) becomes

$$\sigma_{\text{true}}(D_{\text{true}}^{n_{\text{equiv}}}, p_{\text{true}}) = \sigma_{\text{true}}(D_{\text{gen}}^{n_{\text{gen}}}, p_{\text{true}}). \quad (12)$$

We refer to this approach as averaging because it does not resolve features in V and instead averages over the given volume.

3.1 Metric extrapolation

For $p_{\text{true}} = p_{\text{gen}}$, the quantity $\sigma_{\text{true}}(D_{\text{gen}}^{n_{\text{gen}}}, p_{\text{true}})$ will capture only the statistical fluctuations and will vanish for an infinitely large sample $D_{\text{gen}}^{n_{\text{gen}}}$. If $p_{\text{true}} \neq p_{\text{gen}}$, this measure of the deviation also includes a mismodeling contribution, which is independent of the number of sampled events,

$$\begin{aligned} \lim_{n_{\text{gen}} \rightarrow \infty} \sigma_{\text{stat}}(n_{\text{gen}}) &= 0 \\ \lim_{n_{\text{gen}} \rightarrow \infty} \sigma_{\text{model}}(p_{\text{gen}}, p_{\text{true}}) &= \text{const.} \end{aligned} \quad (13)$$

The scaling of σ_{stat} is described by classical statistics. It follows a binomial distribution and can be extrapolated for $n_{\text{gen}} \gg n_{\text{train}}$ based on the finite training dataset. Using the standard deviation of the binomial distribution, the left-hand side of Eq. (12) takes the form

$$\sigma_{\text{true}}^2(D_{\text{true}}^{n_{\text{equiv}}}, p_{\text{true}}) = \sigma_{\text{stat}}^2(n_{\text{equiv}}) \simeq \frac{\bar{I}(D_{\text{true}}^{n_{\text{train}}})[1 - \bar{I}(D_{\text{true}}^{n_{\text{train}}})]}{n_{\text{equiv}}}. \quad (14)$$

Combined with the right-hand side of Eq. (11), this gives us the extrapolated form of the implicit amplification condition for n_{equiv} as in Eq. (12), assuming that n_{gen} is large enough to neglect $\sigma_{\text{stat}}(n_{\text{gen}})$

$$\sigma_{\text{stat}}(n_{\text{equiv}}) = \left[\frac{\bar{I}(D_{\text{true}}^{n_{\text{train}}})[1 - \bar{I}(D_{\text{true}}^{n_{\text{train}}})]}{n_{\text{equiv}}} \right]^{1/2} = \sigma_{\text{model}}(p_{\text{gen}}, p_{\text{true}}), \quad (15)$$

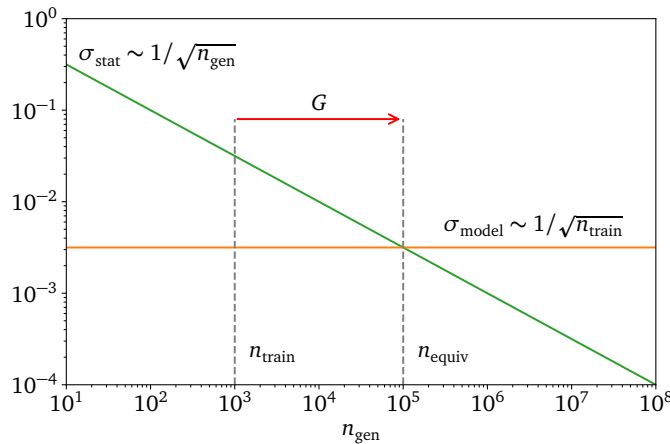


Figure 1: Illustration of the averaging amplification estimate. The statistical uncertainty of the generated dataset is shown in green; the model uncertainty of the generative network is shown in orange.

If we can estimate σ_{model} , we can extract the maximum number of meaningfully generated events, n_{equiv} , and the amplification factor. This procedure is visualized in Fig. 1. For the statistical uncertainty of the generated dataset we use the scaling of σ_{stat} as $1/\sqrt{n_{\text{gen}}}$. The model uncertainty does not depend on n_{gen} and typically scales as $1/\sqrt{n_{\text{train}}}$. The crossing of the lines determines n_{equiv} and hence $G = n_{\text{equiv}}/n_{\text{train}}$.

This averaging amplification factor will depend strongly on the choice of integration region V . A very small integration region will not contain enough events, while using the entire phase space leads to a meaningless result, as $I = 1 = \bar{I}$ by definition. We can split the phase space into n_V non-overlapping regions V_i with $i \in [0, n_V]$ and obtain the combined uncertainty over all V_i as a quadratic sum,

$$\sigma_{\text{stat}}^2 = \sum_i \sigma_{\text{stat}, V_i}^2 \quad \text{and} \quad \sigma_{\text{model}}^2 = \sum_i \sigma_{\text{model}, V_i}^2. \quad (16)$$

Choosing V_i as quantile regions makes this method directly comparable to the approach of Ref. [22], but without knowledge of the true distribution or a holdout dataset.

3.2 1D Gaussian fit

Following Eq. (15), the key step in estimating n_{equiv} is to approximate σ_{model} . To illustrate how this can be achieved, we first examine a 1-dimensional unit Gaussian, where we know the true distribution

$$p_{\text{true}}(x) = \mathcal{N}(x; 0, 1), \quad (17)$$

In place of a generative network, we use a unit-width Gaussian with variable mean $\hat{\mu}$,

$$f(x, \hat{\mu}) = \frac{1}{\sqrt{2\pi}} e^{(x-\hat{\mu})^2/2}, \quad (18)$$

For this 1D Gaussian, a maximum-likelihood fit is equivalent to calculating the mean and standard deviation on the fit data. This means the distribution of $\hat{\mu}$ across multiple fits follows a Gaussian with width $\sigma_{\hat{\mu}}$,

$$\hat{\mu} \sim \mathcal{N}(\hat{\mu}; 0, \sigma_{\hat{\mu}}) \quad \text{with} \quad \sigma_{\hat{\mu}} = \frac{1}{\sqrt{n_{\text{train}}}}. \quad (19)$$

Using this fitted mean $\hat{\mu}$, we draw n_{gen} points from the fitted Gaussian $\mathcal{N}(x; \hat{\mu}, 1)$, just as from a generative network

$$D_{\text{gen}}^{n_{\text{gen}}} \sim p_{\text{gen}}(x) = \mathcal{N}(x; \hat{\mu}, 1). \quad (20)$$

The phase space region V over which we calculate the averaging amplification factor is defined as the interval $[a, b]$. We compute the integral of the Gaussian as

$$I = \int_a^b dx \mathcal{N}(x; 0, 1) = \frac{1}{2} \left[\text{erf}\left(\frac{b}{\sqrt{2}}\right) - \text{erf}\left(\frac{a}{\sqrt{2}}\right) \right]. \quad (21)$$

Next, we compute the fraction of points in $D_{\text{gen}}^{n_{\text{gen}}}$ within the region V . Given that the number of points in $V = [a, b]$ follows a binomial distribution, the statistical uncertainty from the finite number of points can be approximated as

$$\sigma_{\text{stat}}^2(n_{\text{gen}}) \simeq \frac{I(1-I)}{n_{\text{gen}}} \simeq \frac{I}{n_{\text{gen}}}. \quad (22)$$

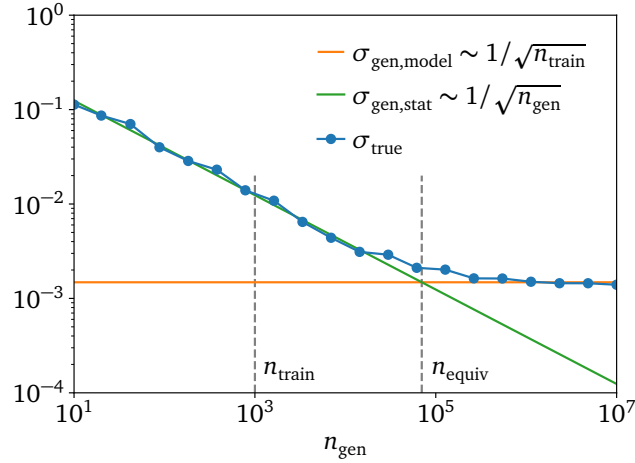


Figure 2: Scaling of the mean quadratic deviation from the true integral value as a function of the number of samples drawn from the fitted Gaussian. The curve points are averaged over 50 independent experiments.

This statistical uncertainty applies to both the training set and the generated set.

The other input to our amplification estimate is the mismodeling uncertainty, in our case from the imperfect fit value $\hat{\mu}$. The exact integral I' over $p_{\text{gen}}(x) = \mathcal{N}(x; \hat{\mu}, 1)$ is

$$\begin{aligned} I' &= \frac{1}{2} \left[\text{erf} \left(\frac{b - \hat{\mu}}{\sqrt{2}} \right) - \text{erf} \left(\frac{a - \hat{\mu}}{\sqrt{2}} \right) \right] \\ &= I + \frac{\hat{\mu}}{\sqrt{2\pi}} \left(e^{-a^2/2} - e^{-b^2/2} \right) + \mathcal{O}(\hat{\mu}^2). \end{aligned} \quad (23)$$

The uncertainty of $\hat{\mu}$ is given in Eq. (19). Using error propagation, we can estimate the modeling uncertainty as

$$\sigma_{\text{model}}(n_{\text{train}}) = \left| \frac{dI'}{d\hat{\mu}} \right| \sigma_{\hat{\mu}} = \frac{1}{\sqrt{2\pi}} \left| e^{-a^2/2} - e^{-b^2/2} \right| \frac{1}{\sqrt{n_{\text{train}}}}. \quad (24)$$

The total generative uncertainty as a function of n_{gen} is then given by

$$\sigma_{\text{true}} = \sqrt{\sigma_{\text{stat}}^2(n_{\text{gen}}) + \sigma_{\text{model}}^2(n_{\text{train}})} \simeq \sqrt{\frac{I(1-I)}{n_{\text{gen}}} + \left| \frac{dI'}{d\hat{\mu}} \right|^2 \frac{1}{n_{\text{train}}}}. \quad (25)$$

In Fig. 2 we show σ_{true} with its two contributions for $V = [0, 0.5]$ and $n_{\text{train}} = 1000$. In this case, we can explicitly evaluate the two uncertainties

$$\sigma_{\text{stat}}(n_{\text{gen}}) = \sqrt{\frac{0.154}{n_{\text{gen}}}} \quad \text{and} \quad \sigma_{\text{model}}(n_{\text{train}}) = \sqrt{\frac{0.0022}{n_{\text{train}}}}. \quad (26)$$

The equivalent number of generated events is obtained from the relation

$$\sigma_{\text{stat}}(n_{\text{equiv}}) \equiv \sigma_{\text{model}}(n_{\text{train}}). \quad (27)$$

Thus, by combining Eq. (26) and Eq. (27), we find

$$n_{\text{equiv}} \simeq \frac{0.154}{0.002} n_{\text{train}} = 70 n_{\text{train}} \quad \text{and} \quad G = \frac{n_{\text{equiv}}}{n_{\text{train}}} \simeq 70. \quad (28)$$

The numerical results for the two uncertainties in Fig. 2, averaged over 50 independent experiments, agree well with the analytic prediction. We can also extract n_{equiv} from the crossing of the two contributions, confirming our previous result $G = 70$.

3.3 Bayesian generative networks

In realistic applications, there are no analytical expressions for the density, therefore we cannot calculate the mismodeling uncertainty using error propagation, like in the previous section. If a large holdout test dataset is available, we can, of course, use it to calculate $I(p_{\text{true}})$. If such a test dataset is not available, we can instead extract σ_{true} using Bayesian Neural Networks (BNNs) [27–30], especially Bayesian generative networks [2, 3, 31]. An alternative which we employ for our physics application are (repulsive) ensembles [20, 21, 32].

BNNs approximate the posterior of the neural network parameters given by the training dataset with an variational inference ansatz,

$$p(\theta|D_{\text{train}}) \approx q(\theta). \quad (29)$$

We can express the density learned by the Bayesian generative network as conditional on the network parameters, $p_{\text{gen}}(x|\theta)$. For the evaluation, we sample N_{BNN} sets of network parameters $\theta_1, \dots, \theta_{N_{\text{BNN}}}$ from $q(\theta)$. For each parameter set, we sample a generated dataset $D_{\text{gen}, \theta_i}^{n_{\text{gen}}}$ and define the fraction of events in V as defined in Eq. (10) and its expectation value over the θ_i as

$$\bar{I}_{\theta_i} = \frac{1}{n_{\text{gen}}} \sum_{x \in D_{\text{gen}, \theta_i}^{n_{\text{gen}}}} \mathbf{1}_{x \in V} \quad \Rightarrow \quad \langle \bar{I} \rangle_{\theta} = \frac{1}{N_{\text{BNN}}} \sum_i \bar{I}_{\theta_i}. \quad (30)$$

If the learned BNN uncertainty is calibrated, the variance of the integral $\langle \bar{I} \rangle_{\theta}$ is equivalent to the deviation $\sigma_{\text{true}}(D_{\text{gen}}^{n_{\text{gen}}}, p_{\text{true}})$,

$$\sigma_{\text{true}}(D_{\text{gen}}^{n_{\text{gen}}}, p_{\text{true}})^2 = \langle \bar{I}^2 \rangle_{\theta} - \langle \bar{I} \rangle_{\theta}^2 = \sigma_{\text{model}}(p_{\text{gen}}, p_{\text{true}})^2 + \sigma_{\text{stat}}(n_{\text{gen}})^2. \quad (31)$$

For large N_{BNN} and large generative networks, drawing a sufficiently large number of generative samples becomes costly. To avoid this, we make use of the fact that the statistical

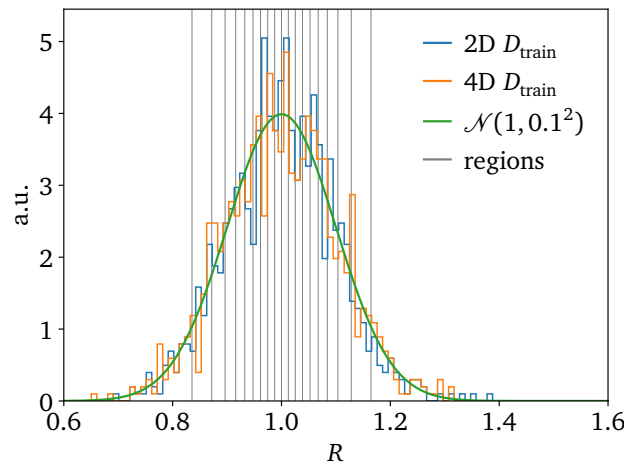


Figure 3: Training data and integral regions for Gaussian ring.

uncertainty can be approximated using

$$\sigma_{\text{stat}}^2(n_{\text{gen}}) \simeq \frac{\langle \bar{I} \rangle_{\theta} (1 - \langle \bar{I} \rangle_{\theta})}{n_{\text{gen}}}. \quad (32)$$

This allows us to extract σ_{model}^2 even if n_{gen} is not large enough to make σ_{stat} negligible, by subtracting σ_{stat}^2 from σ_{true}^2 .

3.4 Gaussian-ring toy data

To validate the extracted amplification factor from BNNs, we use Gaussian ring toy data in two and four dimensions, as described in Section 2. We divide the phase space along the radius direction R into 20 regions, each containing 5% of the events, as shown in Fig. 3. We label the regions sequentially from left to right. For each region, we estimate the integral in Eq. (30) from samples generated with the Bayesian autoregressive transformer and compare it to the true integral values. The resulting amplification curves are shown in Fig. 4. Since σ_{model} is calculated via subtraction, it can become negative due to numerical fluctuations. We do not display these points in the plot. For region 2, shown in the upper panels of Fig. 4, the curves displaying the true and estimated uncertainties σ_{true} overlap, so the BNN learns the uncertainties correctly. The extracted σ_{stat} and σ_{model} also follow the expected scaling behaviors. Consequently, the estimated and true amplification factors agree very well with $G = 2.6$ and $G = 1.9$ for the two- and four-dimensional toy datasets, respectively.

Next, we combine all regions except for the first and the last one in the lower row of Fig. 5. The combination follows Eq. (16), and the estimated σ_{true} is slightly smaller than

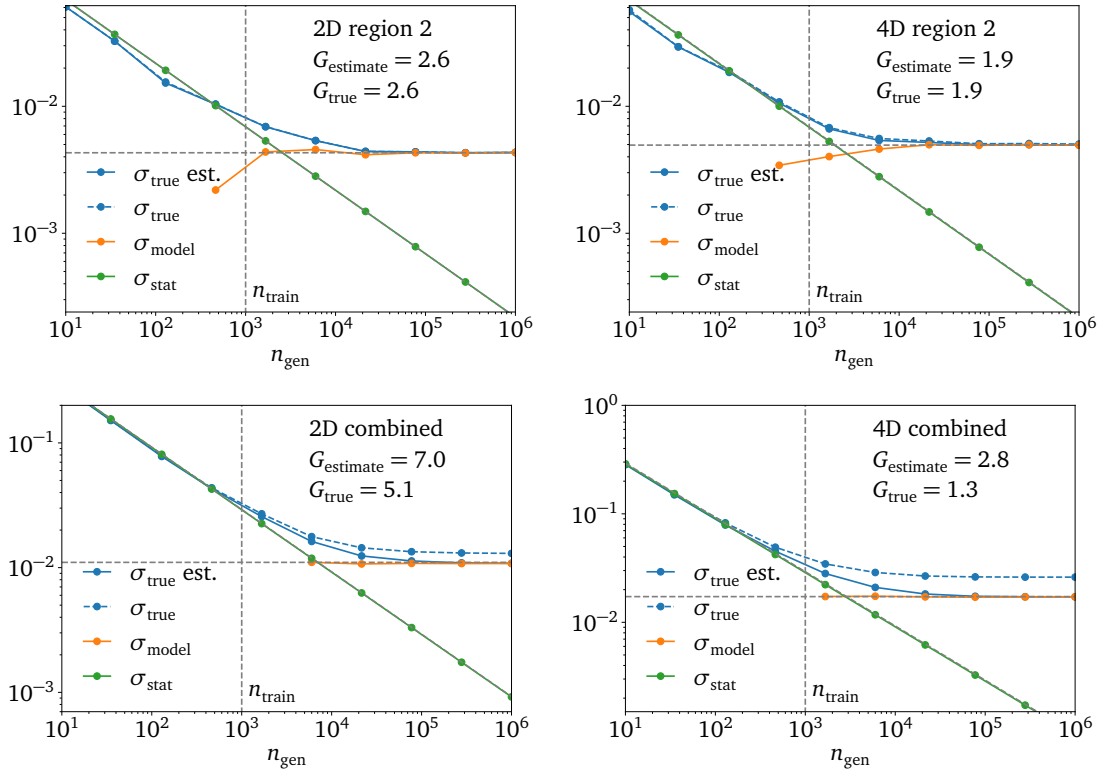


Figure 4: Actual standard deviation and estimated uncertainties for various radial integrals over a Gaussian ring. Left panels: 2D Gaussian ring. Right panels: 4D Gaussian ring.

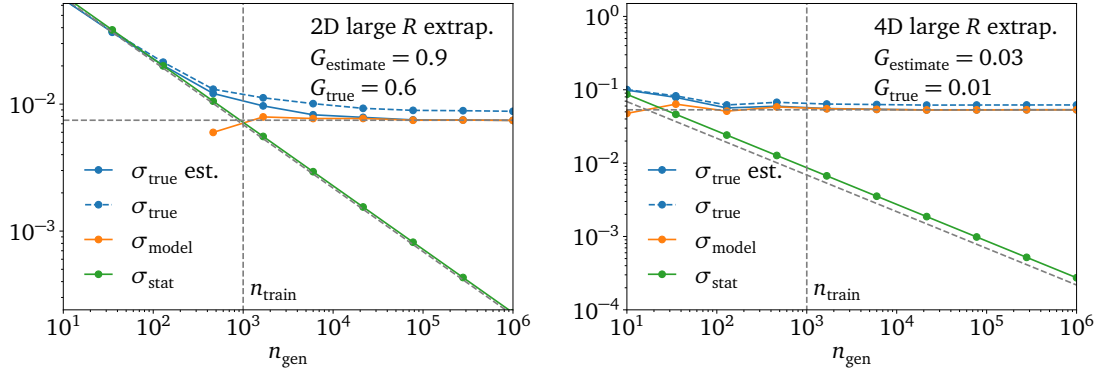


Figure 5: Actual standard deviation and estimated uncertainties for radial integrals, including only regions with large radius R . Left panels: 2D Gaussian ring. Right panels: 4D Gaussian ring.

the true uncertainty. Still, the estimated amplification factors agree reasonably well with the true factors. In the two-dimensional case, the amplification factor is $G \approx 7$, in the more challenging 4D case, we find $G \approx 2.8$. The final result deviates from the true value $G \approx 1.3$ more significantly.

Finally, we specifically study region 20, the tail of the radial distribution. The estimated σ_{true} again tracks the true σ_{true} , but the agreement is worse than in region 2. The predicted amplification factors in region 20 are smaller than one for two dimensions and close to zero for four dimensions. This means the generative network does not learn the underlying density correctly in the low-statistics tails. Crucially, our averaging approach also predicts this amplification failure correctly.

4 Differential amplification factor

In Eq. (3), we introduce amplification based on a metric $M(D, p(x))$ that quantifies the statistical distance between a set of samples D and a probability distribution $p(x)$. In Section 3, our averaging amplification estimate defines this distance as the mean over a phase-space region V , introducing a finite resolution.

Differential amplification is an alternative method that avoids this limited resolution by approximating M with a differential, unbinned test statistic that compares $D_{\text{gen}}^{n_{\text{gen}}}$ to the training data, rather than the true density,

$$M^{\text{test}}(D_{\text{gen}}^{n_{\text{gen}}}, D_{\text{true}}^{n_{\text{train}}}) \simeq M(D_{\text{gen}}^{n_{\text{gen}}}, p_{\text{true}}) \quad \text{with} \quad D_{\text{true}}^{n_{\text{train}}} \sim p_{\text{true}}(x). \quad (33)$$

The implicit definition of n_{equiv} in Eq. (3) now reads

$$M^{\text{test}}(D_{\text{true}}^{n_{\text{equiv}}}, D_{\text{true}}^{n_{\text{train}}}) \equiv M^{\text{test}}(D_{\text{gen}}^{n_{\text{gen}}}, D_{\text{true}}^{n_{\text{train}}}). \quad (34)$$

When the true distribution p_{true} is available implicitly as a large holdout dataset $D_{\text{true}}^{n_{\text{test}}}$, we can obtain an alternative measure of amplification by replacing $D_{\text{true}}^{n_{\text{train}}}$ with this holdout dataset.

This approach requires a two-sample test statistic M^{test} for which the left-hand side of Eq. (34) is known. This is the case if M^{test} has an analytically known asymptotic behavior for both samples drawn from identical distributions. This requirement limits us to univariate test

statistics. While multivariate test statistics exist, e.g. based on maximum mean discrepancy, energy distance, or the earth mover's distance, none of them have a known asymptotic behavior. Further, several univariate test statistics, such as the χ^2 test, Student-t test, and F-test, assume a certain form of the one-dimensional distribution, which we can not guarantee for an arbitrary generative task. Another set of methods, for example the Mann-Whitney U test, only test for differences in the mean or variance of the distributions, but not for the general distribution equality that we want to test. This leaves us with the Kolmogorov-Smirnov (KS) test [33, 34], which is cheap to evaluate and has a known asymptotic behavior.

To perform univariate tests, we need a summary statistic that compresses the high-dimensional phase space information into a one-dimensional variable, which is designed to discriminate between the two datasets. For specific applications, a physically relevant feature might be the best choice. As a general approach, we train a classifier to separate a generated set from the training set. The output of the trained classifier approximates the likelihood ratio for each point in any dataset, describing its agreement with the training data. This likelihood ratio is the most powerful summary statistic according to the Neyman-Pearson lemma, satisfying our criteria for a summary statistic.

4.1 Kolmogorov-Smirnov test

For two one-dimensional datasets D_1, D_2 drawn from the distributions $p_1(x), p_2(x)$, the KS test statistic which we will use for Eq. (33) is defined as

$$M^{\text{KS}}(D_1, D_2) = \sup_y |F(y, D_1) - F(y, D_2)|. \quad (35)$$

The functions F are the empirical cumulative distribution functions (CDF) of the two samples,

$$F(x, D) = \frac{1}{n} \sum_{y_i \in D} \mathbf{1}_{y_i < x} \quad \text{with} \quad |D| = n \quad \text{and} \quad \mathbf{1}_{y_i < x} = \begin{cases} 1 & y_i < x \\ 0 & \text{else} \end{cases}. \quad (36)$$

The KS test statistic has an asymptotic behavior for large $n_{1,2}$ when the two distributions are identical, $p_1(x) = p_2(x)$. The rescaled KS statistic then follows the Kolmogorov distribution $p_K(K)$ [33, 34]

$$\sqrt{\frac{n_1 n_2}{n_1 + n_2}} M^{\text{KS}}(D_1, D_2) = K \sim p_K(K). \quad (37)$$

We will only be interested in the expectation value of our test statistic. This means we can use the expectation value of the Kolmogorov distribution $\langle K \rangle$ and arrive at

$$\sqrt{\frac{n_1 n_2}{n_1 + n_2}} \langle M^{\text{KS}}(D_1, D_2) \rangle = \langle K \rangle = \sqrt{\frac{\pi}{2}} \log 2. \quad (38)$$

We insert this result for two sets drawn from identical distributions in the left-hand side of Eq. (34), giving us the implicit definition for n_{equiv} based on the KS test statistic for large n_{gen} ,

$$\langle K \rangle \sqrt{\frac{n_{\text{equiv}} + n_{\text{train}}}{n_{\text{equiv}} n_{\text{train}}}} \equiv \langle M^{\text{KS}}(D_{\text{gen}}^{n_{\text{gen}}}, D_{\text{true}}^{n_{\text{train}}}) \rangle. \quad (39)$$

We illustrate in Fig. 6 how to extract n_{equiv} and G from this condition. First, we calculate the test statistic $\langle M^{\text{KS}}(D_{\text{gen}}^{n_{\text{gen}}}, D_{\text{true}}^{n_{\text{train}}}) \rangle$ that compares the generated and training datasets for large

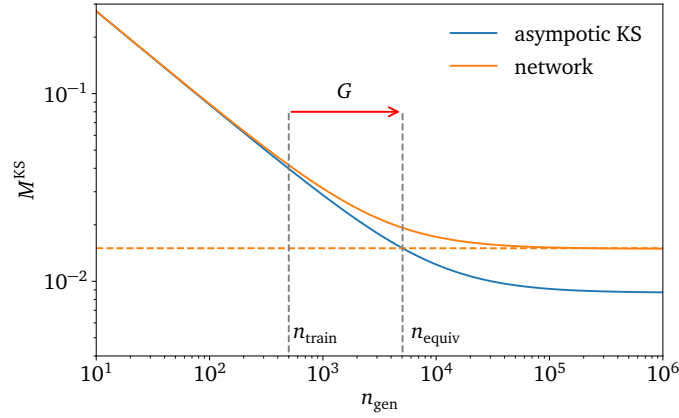


Figure 6: Conceptual sketch of the differential amplification method based on the KS test. The asymptotic behaviour of the KS test is shown in blue; the actual KS test value obtained by comparing the generated and training datasets, in orange.

n_{gen} . Then we identify its crossing point with the asymptotic KS curve. This defines n_{equiv} as the point where Fig. 6 holds.

Fig. 6 also shows the weakness of Eq. (39). For increasing n_{gen} , the asymptotic KS curve flattens and becomes independent of n_{gen} in the limit $n_{\text{gen}} \gg n_{\text{train}}$. This makes it difficult to obtain a precise estimate of large amplification factors. In case we have a large holdout dataset, we can use it in place of the training dataset in M^{KS} to estimate the amplification also for large n_{gen} .

In addition to the mean of the KS test statistics converging to the rescaled mean of the Kolmogorov distribution, we know that the KS test statistic is itself distributed according to a rescaled Kolmogorov distribution for identical distributions. This allows us to quantify deviations from the asymptotic behavior using the confidence levels of the Kolmogorov distribution. Specifically, the Kolmogorov variable K is contained in the interval

$$\langle K \rangle - c(\alpha) < K < \langle K \rangle + c(\alpha) \quad \text{with} \quad c(\alpha) \simeq \sqrt{\frac{1}{2} \ln\left(\frac{2}{\alpha}\right)}. \quad (40)$$

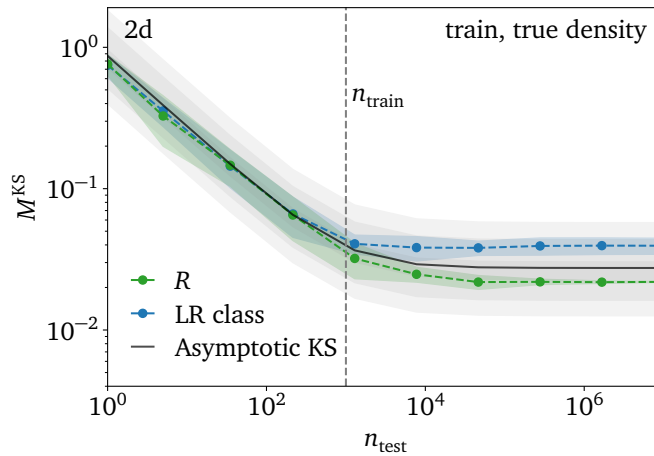


Figure 7: Showing the results for the KS test comparing train vs. an independent test dataset. The uncertainty bands are obtained by averaging over ten classifier samples.

with a probability $1 - \alpha$. We can assign a confidence interval to the amplification factor by replacing $\langle K \rangle$ with $\langle K \rangle \pm c(\alpha)$.

4.2 Gaussian-ring toy data

To estimate differential amplification using the KS test, we again resort to the Gaussian ring toy data introduced in [Section 2](#). We use the two- and four-dimensional versions. For training, we use 10^3 points, while the generated datasets contain up to 10^7 points. The KS test is evaluated for three different summary statistics:

1. R : radius of the Gaussian ring;
2. LR class: likelihood ratio of a classifier trained to distinguish training and generated data;
3. LR truth: true likelihood ratio.

First, we test the consistency of the KS test in [Fig. 7](#) by comparing the training dataset with 1000 points against an independent test dataset of variable size. Both datasets are drawn from the truth distribution, so we expect the KS statistic to follow [Eq. \(39\)](#). This asymptotic behavior is shown as a solid black line. The gray bands indicate the one- to three-sigma intervals of the Kolmogorov distribution. We evaluate the KS test on LR class and R , but not on LR truth, because it is equal for both samples by construction. We estimate uncertainties on the KS statistic using ten independent Bayesian network samples and classifier trainings. Both curves

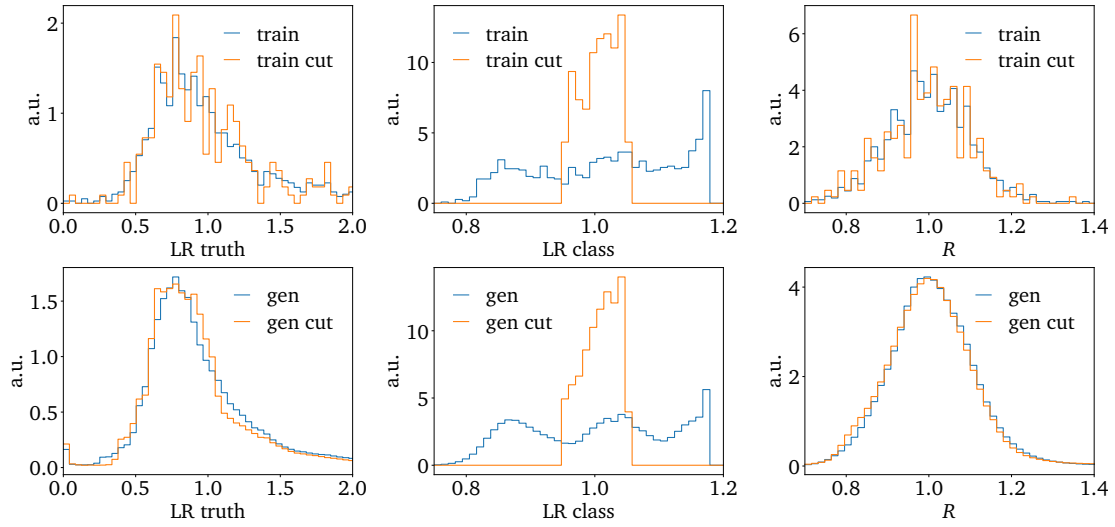


Figure 8: LR truth, LR class and R distributions of the training and generated 2D Gaussian ring data datasets. The blue line represents the results for the full dataset, the orange line the results after removing the largest and smallest classifier weights.

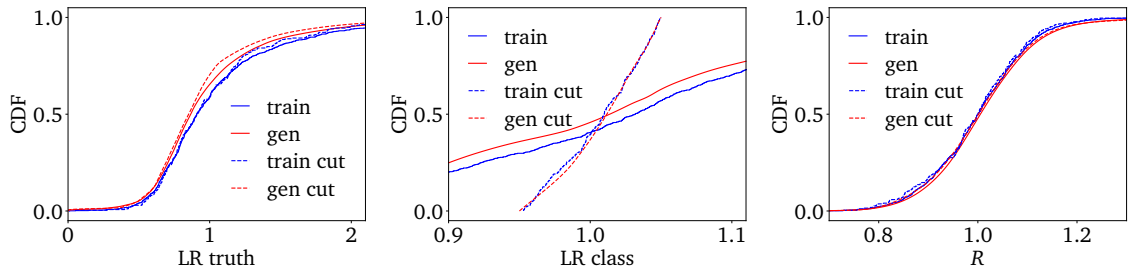


Figure 9: Empirical CDF for LR class, LR truth, and the radius R .

follow the asymptotic KS curve, so the KS test, as expected, is unable to distinguish between the datasets.

Next, we investigate the one-dimensional summary statistics on which the KS test is based. In addition to the full datasets we also define cut datasets, where all events with a likelihood ratio outside $0.95 \dots 1.05$ are removed. This uses the likelihoods to refine the generated set, similar to using classifier-based likelihood ratios for generative improvement [35]. The corresponding histograms for the training and test datasets are shown in Fig. 8. The upper panels show the training datasets, the lower panels the full generated dataset. The training and generated datasets are in good agreement, up to numerical fluctuations.

The empirical CDFs, on which the KS test is based, are shown in Fig. 9. Comparing the CDFs of the training and generated datasets, we see small differences which the KS test is sensitive to. Among the three summary statistics, the smallest difference appears for the R observable, where all angular dependencies are ignored. In the left and middle panels, we also see that cutting on the likelihood ratio reduces the differences between the cumulative distributions.

We study differential amplification in Fig. 10. We compute the KS test statistics between the training dataset and differently-sized subsets of the generated data. As in Section 3, we remove the extrapolation regions for small and high R here, as indicated in the plots.

The upper left panel of Fig. 10 shows that the selected summary statistic affects the pre-

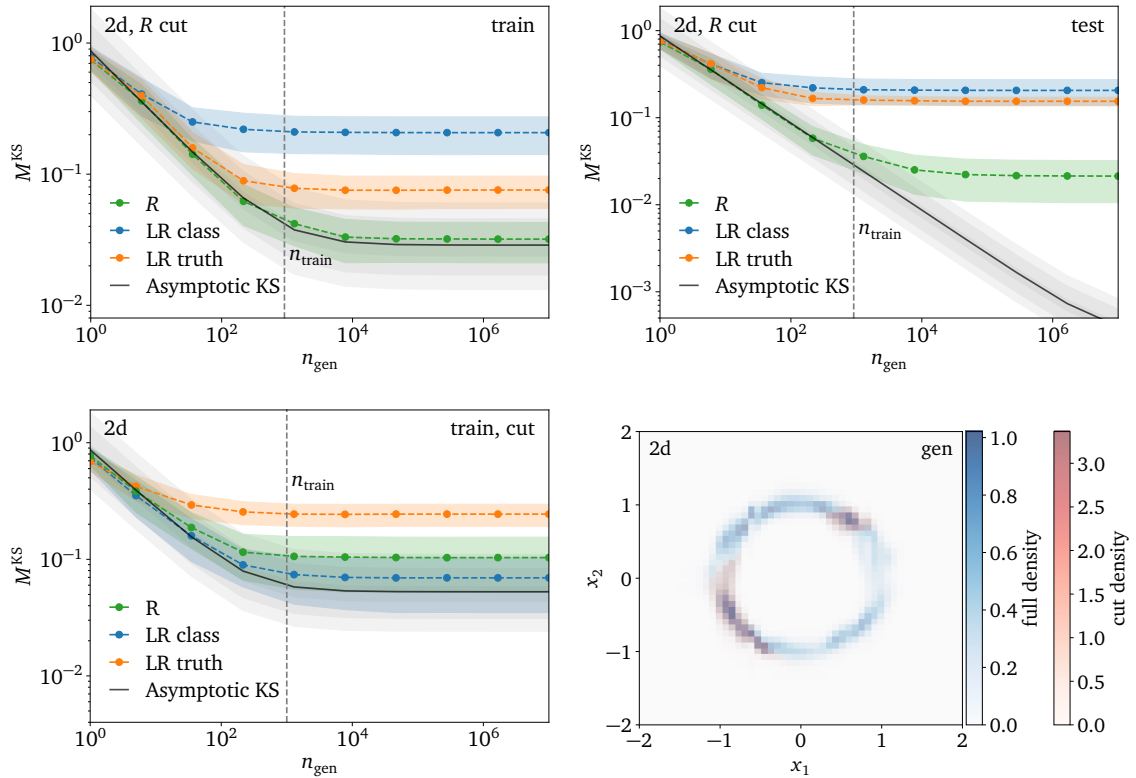


Figure 10: KS test results for a 2D Gaussian toy data, with uncertainties based on 50 samples from the BNN. Upper left: KS test statistic as a function of n_{gen} comparing different one-dimensional summary statistics. Upper right: same but compared to a large holdout test dataset. Lower left: same as upper left, but instead of removing the extrapolation regions, all events for which the classifier score outside $0.95 \dots 1.05$ are removed. Lower right: distribution of all points (blue) and cut points (red) for the generated dataset.

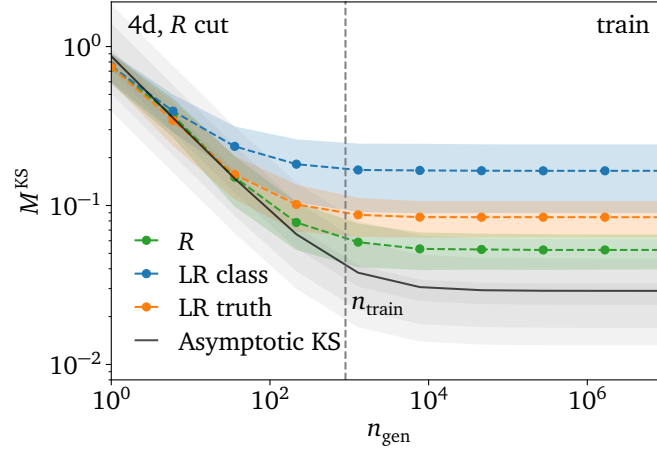


Figure 11: KS test results for a 4D Gaussian toy data. The KS test statistic is shown as a function of n_{gen} comparing different one-dimensional summary statistics.

dicted amplification behavior. Both likelihood ratio based summary statistics do not show any amplification, while we obtain $G \simeq 22$ for the R summary statistic. This behavior is explained by the fact that the radius measure is only sensitive to deviations in the radius distribution, while the two classifier scores are sensitive to any discrepancies. Both amplification estimates are valid, but describe different levels of detail. The upper right panel of Fig. 10 instead compares the generated dataset to a large holdout dataset drawn from the truth distribution. This serves as a cross-check, comparable to Refs. [36, 37], and is not feasible for realistic applications. The amplification behavior is the same as in the left panel. As the large test dataset provides us with a steep asymptotic KS value for large n_{gen} , the amplification values can be determined more reliably.

In the lower left panel of Fig. 10, we present the KS test results on the refined generative set, excluding classifier likelihood ratios that deviate significantly from one. The location of these excluded events is shown in the lower right panel of Fig. 10. The most notable effect is that we now observe a higher amplification factor for the classifier-based KS test. This confirms the validity of our likelihood-ratio-based KS test. The effects of the cut on the KS values for the true likelihood ratio are minimal, due to imperfect training of the classifier.

Finally, we show the results for the standard KS test for the 4D Gaussian ring in Fig. 11. We observe similar trends to those in the 2D case. The radius summary statistic again yields larger amplification factors than the likelihood ratio-based summary statistics. However, the classifier and the true likelihood results now agree within their uncertainties, indicating that the 4D classifier is well-trained. The radius summary statistic does not show amplification anymore, because learning it precisely in this high-dimensional problem is a challenge for the generative network. These findings are in line with previous tests on higher-dimensional Gaussian rings [22].

5 Top pair production

After validating our two ways to estimate amplification on toy datasets, we turn to the generation of reconstruction-level events with two hadronically decaying tops and additional jets.

Datasets

We use top pair events [6] from MADGRAPH5_AMC@NLO 3.5.1 [38]. We use PYTHIA8 [39] for the parton shower and hadronization. The detector simulation is performed with DELPHES [17] using the default ATLAS card. The jets are reconstructed using an anti- k_T algorithm with $R = 0.4$ via FASTJET [40]. As phase-space cuts we employ

$$p_{T,j} > 22 \text{ GeV} \quad \Delta R_{jj} > 0.5 \quad |\eta_j| < 5 \quad N_b = 2. \quad (41)$$

The top quarks are reconstructed using a χ^2 algorithm [41], and all identical particles are sorted by their transverse momentum. We use two datasets with different additional jet multiplicities and the following number of events

$$\begin{aligned} t\bar{t} + 0j : \quad & n_{\text{train}} \sim 5 \cdot 10^5 & n_{\text{test}} \sim 8 \cdot 10^6 \\ t\bar{t} + 4j : \quad & n_{\text{train}} \sim 2 \cdot 10^5 & n_{\text{test}} \sim 2 \cdot 10^5. \end{aligned} \quad (42)$$

Generative networks

Instead of the autoregressive generative network used for the toy studies, we use high-performance event generation networks. Conditional flow matching (CFM) generators with the Lorentz-equivariant L-GATr and LLoCa-Transformers define the state of the art [5, 6]. We also employ a vanilla transformer to quantify the gains from Lorentz equivariance.

CFM generators encode phase space densities $p(x_0)$ sampled from a given latent distribution $p_{\text{latent}}(x_1)$. The continuous transition $x(t)$ is described either by an ordinary differential equation (ODE) or by a continuity equation,

$$\frac{dx(t)}{dt} = v(x(t), t) \quad \text{or} \quad \frac{\partial \rho(x, t)}{\partial t} = -\nabla_x [v(x(t), t) p(x(t), t)], \quad (43)$$

with the same velocity $v(x(t), t)$. The time parametrizes the transition from the latent distribution to the phase space distribution,

$$p(x, t) \rightarrow \begin{cases} p(x) & t \rightarrow 0 \\ p_{\text{latent}}(x) = \mathcal{N}(x; 0, 1) & t \rightarrow 1, \end{cases} \quad (44)$$

The learned velocity field

$$v_\theta(x(t), t) \approx v(x(t), t) \quad (45)$$

allows us to generate events using an ODE solver.

In principle, any network architecture can be used to encode the velocity field. LHC events at reconstruction level respect a rotational $\text{SO}(2)$ symmetry around the beam axis. Embedding it in the velocity network boosts the network performance. The L-GATr [5, 42] and LLoCa-Transformers [6, 43] implement the larger Lorentz symmetry group. Therefore, we also need to incorporate learned symmetry breaking [5, 6].

To estimate a learned (statistical) uncertainty for the generated data, we use ensembling instead of Bayesian Networks [20, 21, 30, 32, 44, 45]. They include 10 independently trained generative networks for each of the three architectures. While formally a repulsive interaction between the ensemble members is needed to guarantee convergence to the true posterior [44], this repulsive kernel can be neglected for large enough training datasets [21].

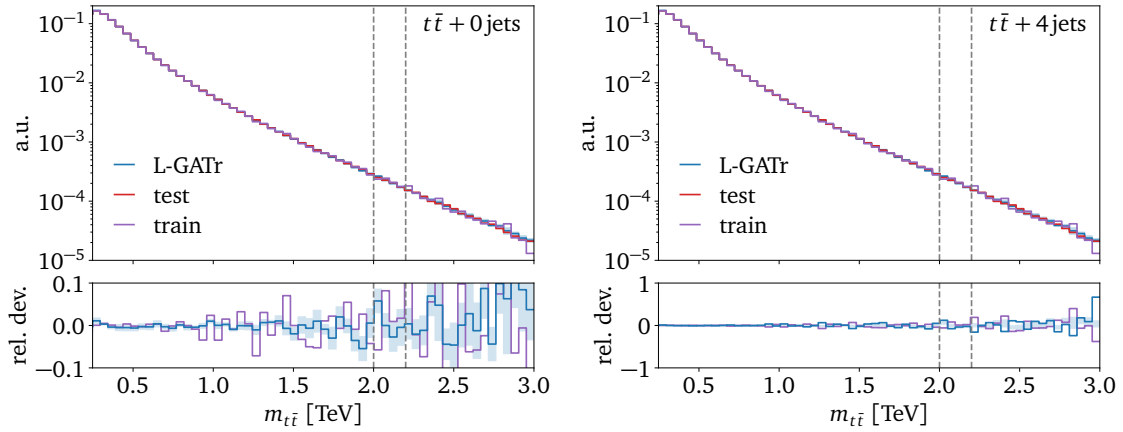


Figure 12: Left: di-top mass from the training and test datasets (upper), and the relative deviation to the test distribution (lower). We also show distributions from the L-GATr CFM network. The colored band indicates the standard deviation around the mean as predicted by the trained NN ensemble. Right: same as left, but for $t\bar{t} + 4$ jets.

5.1 Averaging amplification

We start with the averaging amplification estimate, focusing on a specific $m_{t\bar{t}}$ range. The distributions of the training and test datasets are shown in Fig. 12, for $t\bar{t} + 0$ jets (left) and $t\bar{t} + 4$ jets (right), compared to the L-GATr generator. We also indicate the chosen phase-space region

$$2 \text{ TeV} \leq m_{t\bar{t}} \leq 2.2 \text{ TeV} . \quad (46)$$

For $t\bar{t} + 0$ jets production, we see that the test dataset is, expectedly, noisier than the training dataset in the tail of the distribution. This is also reflected in the L-GATr results, for which we observe a growing spread of the ensemble with increasing $m_{t\bar{t}}$. The behavior is similar for $t\bar{t} + 4$ jets production. Since the size of the test dataset is much smaller, we observe increasing noise for smaller $m_{t\bar{t}}$ values. The L-GATr distributions remain stable over the entire $m_{t\bar{t}}$ range.

Following Section 3, we estimate σ_{true} for the generative networks within this phase-space

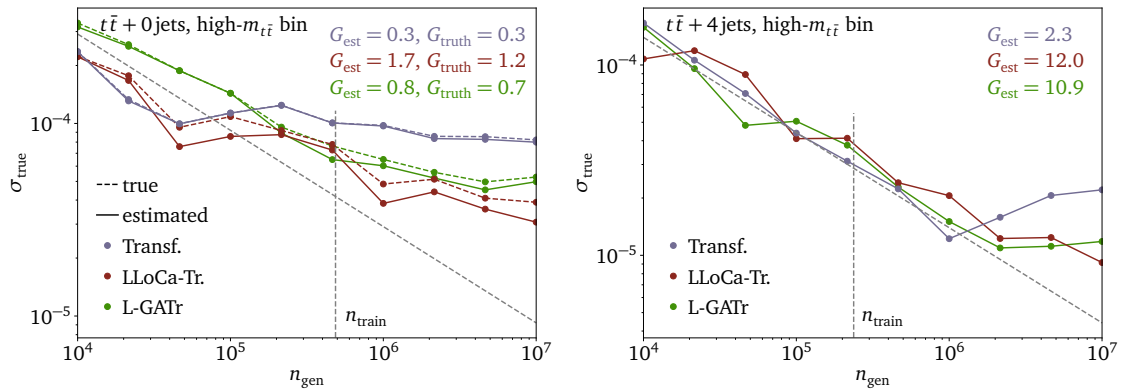


Figure 13: Left: averaging amplification test for $t\bar{t}$ production using three different $t\bar{t}$ event generators. The integral is computed in the region $2 \text{ TeV} \leq m_{t\bar{t}} \leq 2.2 \text{ TeV}$. Right: same as left for $t\bar{t} + 4$ jets production. No “true” curves are shown, as the statistical uncertainty of the test dataset is too high.

region. For $t\bar{t} + 0\text{jets}$ production, we can predict the true integral to $8 \cdot 10^{-4} \pm 1 \cdot 10^{-5}$, a precision sufficient to validate our averaging amplification results. In Fig. 13, we illustrate the averaging estimate for $t\bar{t} + 0\text{jets}$ in the left panel. All three architectures show good agreement between the estimated and true uncertainties. For the transformer and L-GATr architectures, the agreement is nearly perfect. For the LLoCa-Transformer, we observe slight deviations, but within the expected range from the ensemble with its 10 runs. We can also compare the performance of the three architectures. For the standard transformer, we do not observe amplification, corresponding to $G < 1$. The L-GATr generator network does slightly better, with $G \lesssim 1$. Only the LLoCa-Transformer has a sizeable amplification with $G \gtrsim 1$. All estimated amplification factors are in agreement with the corresponding true values.

In the right panel of Fig. 13 we show the corresponding results for $t\bar{t} + 4\text{jets}$ production. Here, the test dataset is smaller, resulting in an integral estimate $2 \cdot 10^{-4} \pm 3 \cdot 10^{-5}$. This limited precision is not sufficient for a good validation. The averaging amplification estimates suggest that all architectures amplify the training dataset in this phase space region. Comparing their performances, the base transformer is the weakest, although still achieving $G > 1$. The LLoCa-Transformer and L-GATr both reach significant amplification factors $G \sim 10$.

5.2 Differential amplification

As an alternative, we also employ our differential amplification estimate for all three architectures. As described in Section 4, we employ a neural classifier as the summary statistic, trained on all phase-space features [5, 6].

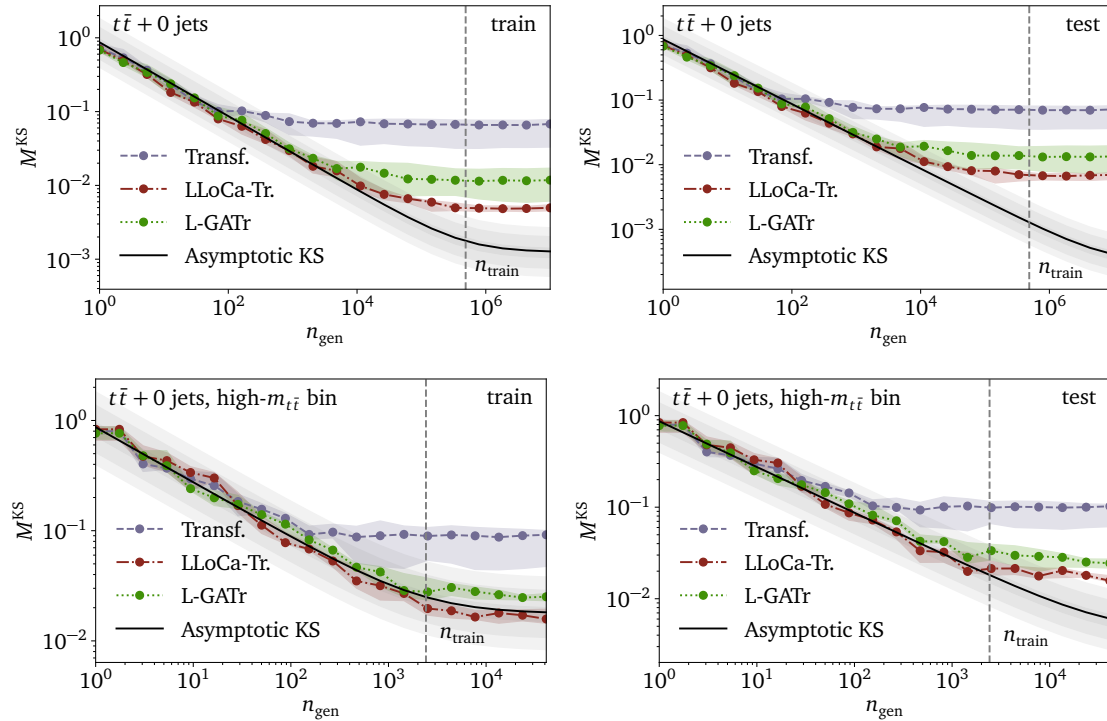


Figure 14: Differential amplification test for the $t\bar{t} + 0\text{jets}$ events for three different architectures. The two panels on the left compare generated and training events, the two panels on the right use a large holdout testing dataset. The top panels use all events for the hypothesis test, whereas the bottom panels use only events in the high- $m_{t\bar{t}}$ bin defined in Eq. (46). The uncertainties are estimated based on ten independent trainings.

The upper left panel of Fig. 14 shows the scaling for $t\bar{t} + 0$ jets production, comparing generated and training datasets. The standard transformer performs notably worse than the two Lorentz-equivariant architectures. For all three generators, the KS statistic already deviates from its asymptotic behavior before the effective number of generated events matches the number of training events. We estimate $G \approx 0.1$ for the two Lorentz-equivariant networks and $G \approx 0.01$ for the standard transformer. These results are confirmed by the larger test dataset in the upper right panel.

Next, we restrict the phase space to the same $m_{t\bar{t}}$ region as in Section 5.1. We show the results of the KS test compared with the training dataset in the lower left panel of Fig. 14. The Lorentz-equivariant architectures again outperform the standard transformer, and their KS test statistics match the asymptotic band over the full range of generated event numbers. This suggests significant amplification. For a more quantitative picture, we again show the test against the large holdout dataset in the lower right panel, confirming amplification with $G \simeq 2$ for the LLoCa-Transformer.

We move on to the $t\bar{t} + 4$ jets case in Fig. 15. In the left panels, we see that the three architectures are now significantly closer in their amplification performance, just like for the averaging amplification estimate. While the differential amplification does not indicate any amplification behavior, individual training of both the LLoCa-Transformer and the L-GATr can reach the asymptotic curve. This suggests that they can probably achieve amplification with a little more fine-tuning.

As before, we now restrict ourselves to the region $2 \text{ TeV} \leq m_{t\bar{t}} \leq 2.2 \text{ TeV}$, where all three KS test statistics follow the expected asymptotic KS behavior, indicating amplification with $G \approx 5$. Without a large holdout dataset, we cannot quantify the possibly larger amplification factor more precisely.

The amplification factors from averaging and differential estimates differ slightly, which is not unexpected. The averaging estimate is based on a phase space region and has no resolution within that region. Even when we combine regions, the resolution will still be limited by their individual sizes. The differential approach does not have resolution issues, so it can pick up very local differences between the datasets. This will result in smaller amplification factors. Our comparison does not prefer one estimate over the other. Instead, it shows the importance of selecting an amplification measure that is appropriate for a given dataset and application.

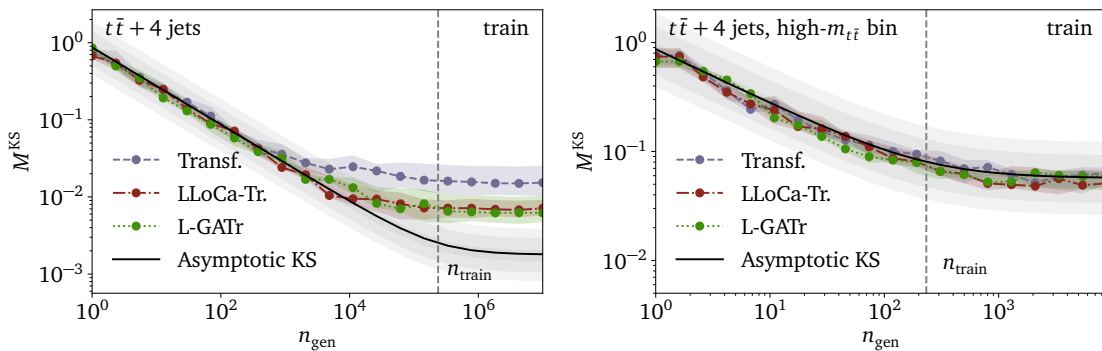


Figure 15: Differential amplification test for the $t\bar{t} + 4$ jets events for three different architectures. The left panel uses all events for the hypothesis test, whereas the right panel uses only events in the high- $m_{t\bar{t}}$ bin defined in Eq. (46). No large test dataset is available for this process. The uncertainties are estimated based on ten independent trainings.

6 Outlook

The main challenge for LHC physics in the coming years is to prepare for the order-of-magnitude increase in data with the HL-LHC. Generative neural networks are key tools to overcome the associated computational obstacles. This means evaluating and controlling their performance is crucial. A fascinating question concerns the amplification factor, the (inverse) ratio of the size of the training dataset and a dataset with statistical power equivalent to the generative network. In this work, we have developed two complementary approaches to estimate the amplification factor without relying on large hold-out test datasets.

First, using an averaging amplification estimate measures the agreement between the integral of the true likelihood and the generative network likelihood for a specific phase-space volume. We demonstrated how this agreement can be estimated using BNNs or network ensembles. Second, we showed how to employ a KS test based on the likelihood ratio to extract the differential amplification factor, which compares the generated dataset to the available truth datasets differentially without averaging.

As a realistic LHC case, we discussed $t\bar{t}$ + jets production. Using our amplification measures, we compared three different generative networks: a transformer, L-GATr, and a LLoCa-Transformer in a CFM generator. For the averaging amplification test on a high- $m_{t\bar{t}}$ region, we confirmed that the Lorentz-equivariant networks lead to amplification in several situations. For the relevant phase space region, we also found evidence for amplification using the differential amplification definition.

Our study provides a systematic framework to quantify the statistical amplification of generative networks in LHC physics. It can easily be applied to tasks beyond the specific toy examples and event generation tasks considered here.

Acknowledgements

We would like to thank Louis Lyons for asking the right question, repeatedly, and this way triggering this study. S.D. is supported by the U.S. Department of Energy (DOE), Office of Science under contract DE-AC02-05CH11231. J.S. is funded by the Carl-Zeiss-Stiftung through the project Model-Based AI: Physical Models and Deep Learning for Imaging and Cancer Treatment. N.E. is funded by the Heidelberg IMPRS *Precision Tests of Fundamental Symmetries*. This research is supported through the KISS consortium (05D2022) funded by the German Federal Ministry of Education and Research BMBF in the ErUM-Data action plan, by the Deutsche Forschungsgemeinschaft (DFG, German Research Foundation) under grant 396021762 – TRR 257: *Particle Physics Phenomenology after the Higgs Discovery*, and through Germany’s Excellence Strategy EXC 2181/1 – 390900948 (the *Heidelberg STRUCTURES Excellence Cluster*). Finally, we would like to thank the Baden-Württemberg Stiftung for financing through the program *Internationale Spitzenforschung*, project *Uncertainties – Teaching AI its Limits* (BWST_ISF2020-010).

References

- [1] A. Butter, T. Plehn, and R. Winterhalder, *How to GAN LHC Events*, *SciPost Phys.* **7** (2019) 6, 075, [arXiv:1907.03764 \[hep-ph\]](#).
- [2] A. Butter, T. Heimel, S. Hummerich, T. Krebs, T. Plehn, A. Rousselot, and S. Vent, *Generative networks for precision enthusiasts*, *SciPost Phys.* **14** (2023) 4, 078, [arXiv:2110.13632 \[hep-ph\]](#).
- [3] A. Butter, N. Huetsch, S. Palacios Schweitzer, T. Plehn, P. Sorrenson, and J. Spinner, *Jet diffusion versus JetGPT – Modern networks for the LHC*, *SciPost Phys. Core* **8** (2025) 026, [arXiv:2305.10475 \[hep-ph\]](#).
- [4] A. Butter, F. Charton, J. M. Villadamigo, A. Ore, T. Plehn, and J. Spinner, *Extrapolating Jet Radiation with Autoregressive Transformers*, [arXiv:2412.12074 \[hep-ph\]](#).
- [5] J. Brehmer, V. Bresó, P. de Haan, T. Plehn, H. Qu, J. Spinner, and J. Thaler, *A Lorentz-Equivariant Transformer for All of the LHC*, [arXiv:2411.00446 \[hep-ph\]](#).
- [6] L. Favaro, G. Gerhartz, F. A. Hamprecht, P. Lippmann, S. Pitz, T. Plehn, H. Qu, and J. Spinner, *Lorentz-Equivariance without Limitations*, [arXiv:2508.14898 \[hep-ph\]](#).
- [7] J. Chan, X. Ju, A. Kania, B. Nachman, V. Sangli, and A. Siodmok, *Fitting a deep generative hadronization model*, *JHEP* **09** (2023) 084, [arXiv:2305.17169 \[hep-ph\]](#).
- [8] P. Ilten, T. Menzo, A. Youssef, and J. Zupan, *Modeling hadronization using machine learning*, *SciPost Phys.* **14** (2023) 3, 027, [arXiv:2203.04983 \[hep-ph\]](#).
- [9] O. Amram *et al.*, *CaloChallenge 2022: A Community Challenge for Fast Calorimeter Simulation*, [arXiv:2410.21611 \[physics.ins-det\]](#).
- [10] L. Favaro, A. Ore, S. P. Schweitzer, and T. Plehn, *CaloDREAM – Detector Response Emulation via Attentive flow Matching*, *SciPost Phys.* **18** (2025) 088, [arXiv:2405.09629 \[hep-ph\]](#).
- [11] J. Q. Toledo-Marin *et al.*, *Conditioned quantum-assisted deep generative surrogate for particle-binary vector indicating the calorimeter interactions*, *npj Quantum Inf.* **11** (2025) 1, 114, [arXiv:2410.22870 \[cs.LG\]](#).
- [12] C. Krause, D. Wang, and R. Winterhalder, *BitHEP – The Limits of Low-Precision ML in HEP*, [arXiv:2504.03387 \[hep-ph\]](#).
- [13] T. Buss, F. Gaede, G. Kasieczka, A. Korol, K. Krüger, P. McKeown, and M. Mozzanica, *CaloHadronic: a diffusion model for the generation of hadronic showers*, [arXiv:2506.21720 \[physics.ins-det\]](#).
- [14] T. Heimel, R. Winterhalder, A. Butter, J. Isaacson, C. Krause, F. Maltoni, O. Mattelaer, and T. Plehn, *MadNIS – Neural Multi-Channel Importance Sampling*, [arXiv:2212.06172 \[hep-ph\]](#).
- [15] T. Heimel, N. Huetsch, F. Maltoni, O. Mattelaer, T. Plehn, and R. Winterhalder, *The MadNIS reloaded*, *SciPost Phys.* **17** (2024) 1, 023, [arXiv:2311.01548 \[hep-ph\]](#).
- [16] T. Heimel, O. Mattelaer, T. Plehn, and R. Winterhalder, *Differentiable MadNIS-Lite*, *SciPost Phys.* **18** (2025) 1, 017, [arXiv:2408.01486 \[hep-ph\]](#).

- [17] DELPHES 3, J. de Favereau, C. Delaere, P. Demin, A. Giammanco, V. Lemaître, A. Mertens, and M. Selvaggi, *DELPHES 3, A modular framework for fast simulation of a generic collider experiment*, *JHEP* **02** (2014) 057, [arXiv:1307.6346 \[hep-ex\]](#).
- [18] F. Bishara and M. Montull, *(Machine) Learning Amplitudes for Faster Event Generation*, [arXiv:1912.11055 \[hep-ph\]](#).
- [19] S. Badger, A. Butter, M. Luchmann, S. Pitz, and T. Plehn, *Loop amplitudes from precision networks*, *SciPost Phys. Core* **6** (2023) 034, [arXiv:2206.14831 \[hep-ph\]](#).
- [20] H. Bahl, N. Elmer, L. Favaro, M. Haußmann, T. Plehn, and R. Winterhalder, *Accurate Surrogate Amplitudes with Calibrated Uncertainties*, [arXiv:2412.12069 \[hep-ph\]](#).
- [21] H. Bahl, N. Elmer, T. Plehn, and R. Winterhalder, *Amplitude Uncertainties Everywhere All at Once*, [arXiv:2509.00155 \[hep-ph\]](#).
- [22] A. Butter, S. Diefenbacher, G. Kasieczka, B. Nachman, and T. Plehn, *GANplifying event samples*, *SciPost Phys.* **10** (2021) 6, 139, [arXiv:2008.06545 \[hep-ph\]](#).
- [23] S. J. Watts and L. Crow, *An information theoretic limit to data amplification*, *Mach. Learn. Sci. Tech.* **6** (2025) 2, 025046, [arXiv:2412.18041 \[stat.ML\]](#).
- [24] S. Bieringer, S. Diefenbacher, G. Kasieczka, and M. Trabs, *Calibrating Bayesian generative machine learning for Bayesiamplification*, *Mach. Learn. Sci. Tech.* **5** (2024) 4, 045044, [arXiv:2408.00838 \[cs.LG\]](#).
- [25] S. Bieringer, A. Butter, S. Diefenbacher, E. Eren, F. Gaede, D. Hundhausen, G. Kasieczka, B. Nachman, T. Plehn, and M. Trabs, *Calomplification — the power of generative calorimeter models*, *JINST* **17** (2022) 09, P09028, [arXiv:2202.07352 \[hep-ph\]](#).
- [26] A. Butter, S. Diefenbacher, G. Kasieczka, B. Nachman, and T. Plehn, *GANplifying Event Samples*, [arXiv:2008.06545 \[hep-ph\]](#).
- [27] Y. Gal, *Uncertainty in Deep Learning*. PhD thesis, Cambridge, 2016.
- [28] S. Bollweg, M. Haußmann, G. Kasieczka, M. Luchmann, T. Plehn, and J. Thompson, *Deep-Learning Jets with Uncertainties and More*, *SciPost Phys.* **8** (2020) 1, 006, [arXiv:1904.10004 \[hep-ph\]](#).
- [29] G. Kasieczka, M. Luchmann, F. Otterpohl, and T. Plehn, *Per-Object Systematics using Deep-Learned Calibration*, *SciPost Phys.* **9** (2020) 089, [arXiv:2003.11099 \[hep-ph\]](#).
- [30] ATLAS, G. Aad et al., *Precision calibration of calorimeter signals in the ATLAS experiment using an uncertainty-aware neural network*, [arXiv:2412.04370 \[hep-ex\]](#).
- [31] M. Bellagente, M. Haussmann, M. Luchmann, and T. Plehn, *Understanding Event-Generation Networks via Uncertainties*, *SciPost Phys.* **13** (2022) 1, 003, [arXiv:2104.04543 \[hep-ph\]](#).
- [32] H. Bahl, V. Bresó, G. De Crescenzo, and T. Plehn, *Advancing Tools for Simulation-Based Inference*, [arXiv:2410.07315 \[hep-ph\]](#).
- [33] K. An, *Sulla determinazione empirica di una legge didistribuzione*, *Giorn Dell’inst Ital Degli Att* **4** (1933) 89.
- [34] N. Smirnov, *Table for estimating the goodness of fit of empirical distributions*, *The annals of mathematical statistics* **19** (1948) 2, 279.

- [35] S. Diefenbacher, E. Eren, G. Kasieczka, A. Korol, B. Nachman, and D. Shih, *DCTRGAN: Improving the Precision of Generative Models with Reweighting*, *JINST* **15** (9, 2020) P11004, [arXiv:2009.03796 \[hep-ph\]](#).
- [36] A. Butter, S. Diefenbacher, G. Kasieczka, B. Nachman, and T. Plehn, *GANplifying event samples*, *SciPost Phys.* **10** (2021) 6, 139, [arXiv:2008.06545 \[hep-ph\]](#).
- [37] S. Bieringer, A. Butter, S. Diefenbacher, E. Eren, F. Gaede, D. Hundhausen, G. Kasieczka, B. Nachman, T. Plehn, and M. Trabs, *Calomplification — the power of generative calorimeter models*, *JINST* **17** (2022) 09, P09028, [arXiv:2202.07352 \[hep-ph\]](#).
- [38] J. Alwall, M. Herquet, F. Maltoni, O. Mattelaer, and T. Stelzer, *MadGraph 5 : Going Beyond*, *JHEP* **06** (2011) 128, [arXiv:1106.0522 \[hep-ph\]](#).
- [39] T. Sjöstrand, S. Ask, J. R. Christiansen, R. Corke, N. Desai, P. Ilten, S. Mrenna, S. Prestel, C. O. Rasmussen, and P. Z. Skands, *An introduction to PYTHIA 8.2*, *Comput. Phys. Commun.* **191** (2015) 159, [arXiv:1410.3012 \[hep-ph\]](#).
- [40] M. Cacciari, G. P. Salam, and G. Soyez, *FastJet User Manual*, *Eur. Phys. J. C* **72** (2012) 1896, [arXiv:1111.6097 \[hep-ph\]](#).
- [41] ATLAS, G. Aad et al., *Measurements of top-quark pair single- and double-differential cross-sections in the all-hadronic channel in pp collisions at $\sqrt{s} = 13$ TeV using the ATLAS detector*, *JHEP* **01** (2021) 033, [arXiv:2006.09274 \[hep-ex\]](#).
- [42] J. Spinner, V. Bresó, P. de Haan, T. Plehn, J. Thaler, and J. Brehmer, *Lorentz-Equivariant Geometric Algebra Transformers for High-Energy Physics*, [arXiv:2405.14806 \[physics.data-an\]](#).
- [43] J. Spinner, L. Favaro, P. Lippmann, S. Pitz, G. Gerhartz, T. Plehn, and F. A. Hamprecht, *Lorentz Local Canonicalization: How to Make Any Network Lorentz-Equivariant*, [arXiv:2505.20280 \[stat.ML\]](#).
- [44] F. D’Angelo and V. Fortuin, *Repulsive deep ensembles are bayesian*, [arXiv:2106.11642 \[cs.LG\]](#).
- [45] L. Röver, B. M. Schäfer, and T. Plehn, *PINNferring the Hubble Function with Uncertainties*, [arXiv:2403.13899 \[astro-ph.CO\]](#).